computation

MDPI

Article

Improved Computational Prediction of the Electrochemical Reduction Potential of Twenty 3-Aryl-Quinoxaline-2-Carbonitrile 1,4-Di-N-Oxide Derivatives

Shambhu Bhattarai †, Pradeep Mareta †, Philip W. Crawford, Jonathan M. Kessler and Christina M. Ragain *

Department of Chemistry and Physics, Southeast Missouri State University, Cape Girardeau, MO 63701, USA
* Correspondence: cragain@semo.edu; Tel.: +1-573-561-2373
† These authors contributed equally to this work.

Abstract: The ability of density functional theory (DFT) using the functional B3LYP with the cc-pVTZ basis set to accurately predict the electrochemical properties of 20 3-aryl-quinoxaline-2-carbonitrile 1,4-di-N-oxide derivatives in dimethylformamide (DMF) was investigated and compared to previous predictions from B3LYP/6-31G and B3LYP/lanl2dz. The B3LYP/cc-pVTZ method was an improvement over the B3LYP/6-31G and B3LYP/lanl2dz methods as it was able to predict the first reduction potential of the diazine ring (wave 1) for all of the 3-aryl-quinoxaline-2-carbonitrile 1,4-di-N-oxide derivatives accurately. The B3LYP/cc-pVTZ predicted electrochemical potentials had a strong correlation to experimental values for wave 1. None of the methods demonstrated the ability to predict the nitro wave reduction potential for derivatives containing a nitro group. B3LYP/cc-pVTZ predicted electrochemical potentials for the second reduction of the diazine ring (wave 2) had a low correlation to the experimental values for the derivatives without a nitro group and no correlation of the derivatives when the nitro group was included in the analysis.

Keywords: quinoxaline-di-N-oxide derivatives; reduction potentials; computation; ab initio; density functional theory; cc-pVTZ

Citation: Bhattarai, S.; Mareta, P.; Crawford, P.W.; Kessler, J.M.; Ragain, C.M. Improved Computational Prediction of the Electrochemical Reduction Potential of Twenty 3-Aryl-Quinoxaline-2-Carbonitrile 1,4-Di-N-Oxide Derivatives. *Computation* **2023**, *11*, 9. https://doi.org/10.3390/computation11010009

Received: 2 December 2022
Revised: 3 January 2023
Accepted: 4 January 2023
Published: 7 January 2023

1. Introduction

Research into quinoxaline 1,4-di-N-oxide derivatives is of interest to the pharmaceutical community, as these compounds have been associated with a wide range of bioactivities including anti-tumor, anti-cancer, antimicrobial, antiparasitic and antioxidant [1–13]. As a result, a significant number of new quinoxaline 1,4-di-N-oxides are designed, synthesized, and tested for biological properties each year [14]. While the exact mechanism for the bioactivities is not known for most quinoxaline 1,4-di-N-oxide derivatives, it has been observed that bioactivity is often linked to the ease of reduction for homologous derivative series [9,15,16]. For some quinoxaline 1,4-di-N-oxide derivatives, it has been shown that they produce a free-radical species capable of cleaving DNA under hypoxic conditions [17,18]. The formation of the free radical is believed to cause cellular oxidative damage and is presumed to be a common bioactivity mechanism for the quinoxaline 1,4-di-N-oxide derivatives [17,18]. Figure 1 shows the first (wave 1) and second (wave 2) reductions of the diazine ring in the parent 3-phenyl-quinoxaline-2-carbonitrile 1,4-di-N-oxide molecule.

The common correlation between the ease of reduction and bioactivity has made understanding the electrochemical reduction potentials of quinoxaline 1,4-di-N-oxide derivatives of interest to the pharmaceutical community. Voltametric techniques are commonly used to experimentally measure the electrochemical reduction potentials of the quinoxaline 1,4-di-N-oxide derivatives. We have proposed that computational techniques can be a powerful tool allowing for the prediction of electrochemical reduction potentials. For quinones and other small organic molecules, computational techniques have been used

to study electrochemical potentials or the highest occupied molecular orbital/lowest unoccupied molecular orbital (HOMO/LUMO) gap [20–24]. For quinoxaline derivatives, computational studies have been used to investigate a wide variety of properties including thermodynamic properties and the impact of substituents on polymerization [20,24–26].

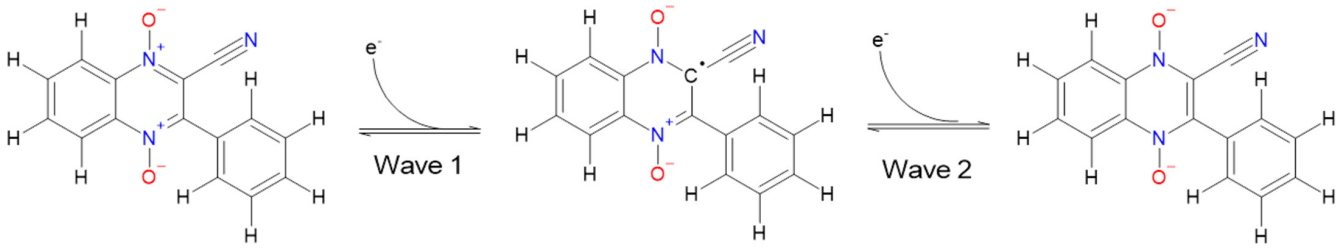

Figure 1. The first reduction (wave 1) and second reduction (wave 2) of the diazine ring in the parent 3-phenyl-quinoxaline-2-carbonitrile 1,4-di-N-oxide, derivative A1. Chemical structures were drawn in ChemSketch FreeWare [19].

In our previous study, we performed calculations using B3LYP/6-31G and B3LYP/lanl2dz methods to predict the electrochemical reduction potentials for a set of 20 3-aryl-quinoxaline-2-carbonitrile 1,4-di-N-oxide derivatives [27]. The 20 3-aryl-quinoxaline-2-carbonitrile 1,4-di-N-oxides were originally synthesized and studied by Sheng et al. for potential anti-tumor properties [28]. The parent molecule structure of the 3-aryl-quinoxaline-2-carbonitrile 1,4-di-N-oxide [27,28] and the list of the substituent groups for each derivative are shown in Table 1. The structures for all 20 derivatives are shown in Figure A1 in the Appendix A with the substituent R1 and R2 groups highlighted. The derivatives can accept two electrons during the first and second reduction of the diazine ring, as shown in Figure 1. Derivatives E1–E4 contain an R2 substituent nitro group, which also undergoes reduction in addition to the diazine ring. The 6-31G and lanl2dz basis sets were demonstrated to have limited usefulness for predicting the reduction potentials for these 3-aryl-quinoxaline-2-carbonitrile 1,4-di-N-oxide derivatives [27]. However, these basis sets could not give realistic predictions for the reduction potentials of the nitro group containing derivatives (Table 1. Compounds E1-E4) [27]. Additionally, B3LYP/6-31G and B3LYP/lanl2dz method led to artificially long C–Cl bond lengths in the trianion or fully reduced structure of the E4 derivative [27]. The bond lengthening caused the Cl to dissociate from the trianion structure when optimized with B3LYP/6-31G [27]. Lanl2dz and 6-31G are both limited basis sets [29,30]. The 6-31G basis set only used six primitive functions. The lanl2dz is a double-zeta basis set without polarization functions. The C–Cl bond distance is likely an artifact of using the limited basis sets without any polarization functions. When the nitro group containing derivatives were removed from the analysis, the predicted electrochemical potentials from these methods had a strong correlation to the experimental potentials for the first reduction of the diazine ring (wave 1) and a poor correlation for the second reduction of the diazine ring (wave 2) [27].

Recently, we investigated the ability of the B3LYP/lanl2dz method to predict the electrochemical reduction potentials for a second set of homologous 1,4-di-N-oxide quinoxaline derivatives. A set of 37 1,4-di-N-oxide quinoxaline-2-carboxamide derivatives [31] was studied. The B3LYP/lanl2dz method was more successful in this new set of derivatives as it was able to accurately predict the electrochemical potentials for all 37 of the derivatives. The B3LYP/lanl2dz predicted electrochemical potentials for the 37 1,4-di-N-oxide quinoxaline-2-carboxamide derivatives had a strong correlation to wave 1 and little to no correlation to wave 2 experimental potentials [31].

In this study, we use the B3LYP/cc-pVTZ method [32] to predict the electrochemical potentials for the 20 3-aryl-quinoxaline-2-carbonitrile 1,4-di-N-oxide derivatives (Table 1) used in our 2019 study [27]. The B3LYP/cc-pVTZ predictions were compared to the experimental data [33] and those previously calculated using the B3LYP/lanl2dz and

B3LYP/6-31G methods [27]. The cc-pVTZ is a triple-zeta basis set [32] and is considered more robust compared to the 6-31G and lanl2dz basis sets used in the 2019 study. The cc-pVTZ basis set is designed to use more functions to describe the valence electrons in the system [32]. For example, the cc-pVTZ basis set uses 30 functions to describe carbon (4s,3p,2d,1f), including 2d and 1f polarization functions. Therefore, the cc-pVTZ basis set would be expected to do a better job in predicting the geometries and energies associated with the anion and dianion systems [34].

Table 1. The structure of the parent 3-aryl-quinoxaline-2-carbonitrile 1,4-di-N-oxide molecule drawn in ChemSketch [19] with the R1 and R2 substituents for each derivative indicated [27,28].

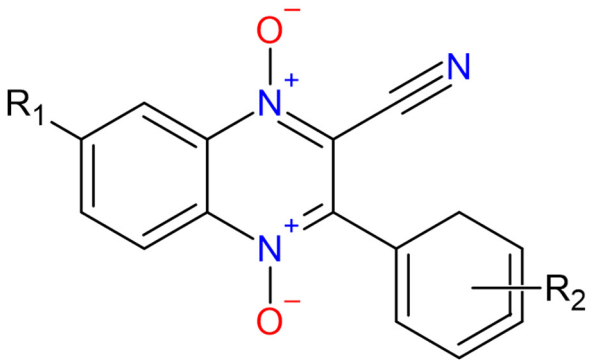

Compound	R_1	R_2
A1	H	H
A2	CH_3	H
A3	OCH_3	H
A4	Cl	H
B1	H	3-CH_3
B2	CH_3	3-CH_3
B3	OCH_3	3-CH_3
B4	Cl	3-CH_3
C1	H	3-Cl
C2	CH_3	3-Cl
C3	OCH_3	3-Cl
C4	Cl	3-Cl
D1	H	4-Br
D2	CH_3	4-Br
D3	OCH_3	4-Br
D4	Cl	4-Br
E1	H	4-NO_2
E2	CH_3	4-NO_2
E3	OCH_3	4-NO_2
E4	Cl	4-NO_2

2. Materials and Methods

2.1. Building the 3-Aryl-quinoxaline-2-carbonitrile 1,4-di-N-oxide Derivatives

A series of structures with varying oxidation states were drawn for each 3-aryl-quinoxaline-2-carbonitrile 1,4-di-N-oxide derivative with the charges specified in the input file using GaussView 5 [35]. For each derivative without a nitro functional group (derivatives A1-D4), three individual structures were previously built [27]; the original neutral molecule, the radical anion product (wave 1 product) and the dianion product (wave 2 product). Figure 2 shows the three individual structures used for derivative A1. For each derivative containing the nitro group (derivatives E1-E4), four structures were previously created [27]; the original neutral molecule, the radical anion product (wave 1 product), the diradical dianion product (nitro wave product), and the radical trianion product (wave 2 product). Figure 3 shows the four structures for E1.

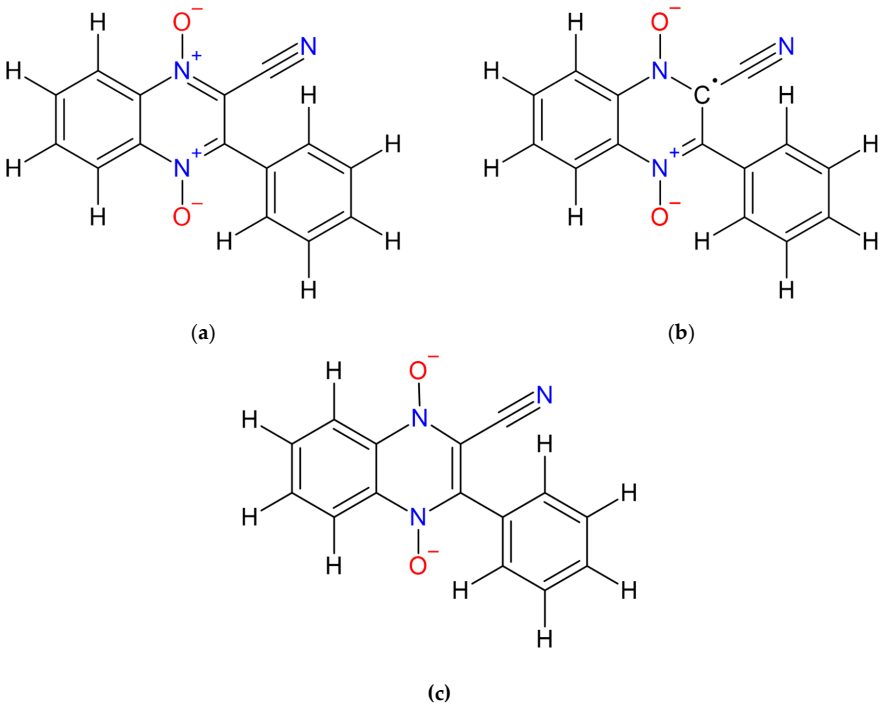

Figure 2. The structure of (**a**) the molecule, (**b**) the anion product from wave 1, and (**c**) the dianion product of wave 2 for derivative A1. Chemical structures drawn in Chemsketch Freeware [19].

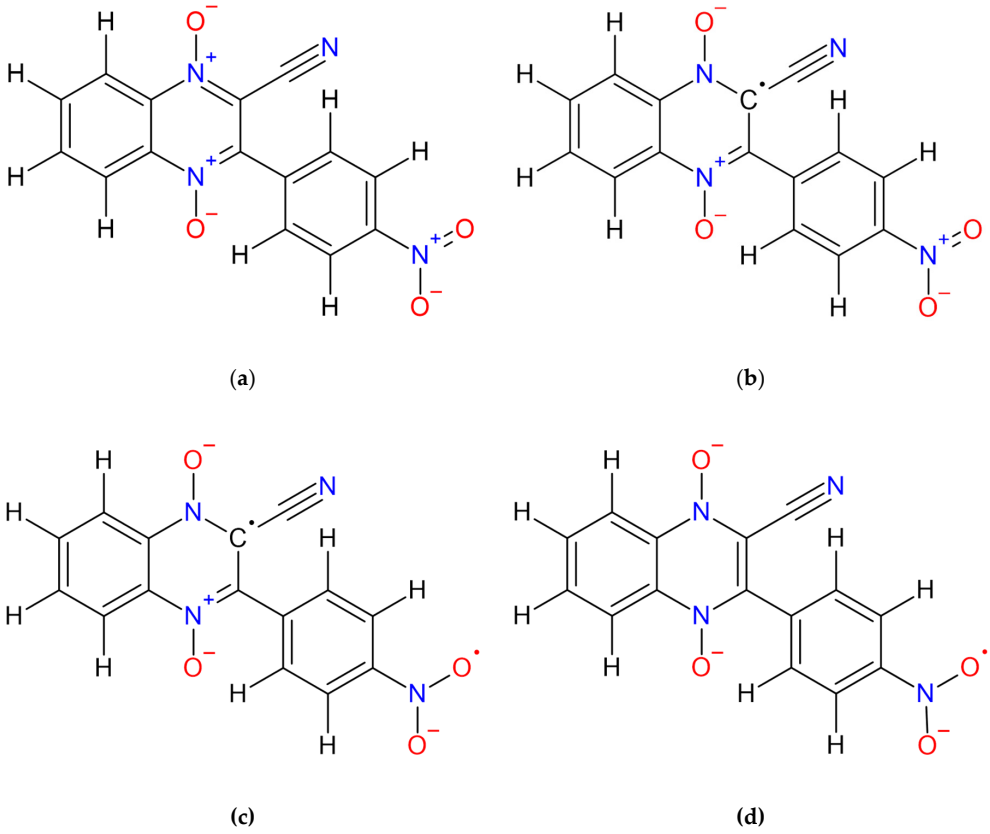

Figure 3. The structure of (**a**) the molecule, (**b**) the radical anion product of wave 1, (**c**) the diradical dianion product of the nitro wave, and (**d**) the radical trianion product of wave 2 for derivative E1. Chemical structures drawn in ChemSketch Freeware [19].

2.2. DFT Calculations

Geometry optimization was performed using density functional theory (DFT) with the functional B3LYP and the cc-pVTZ basis set in Gaussian 09 [36]. The default criteria were used including using the Gaussian 09 default "fine" grid for integrations. Each structure was optimized in the gas phase to determine the lowest energy configuration. Next, to consider thermal contributions, frequency calculations were performed. The gas-phase energy (E_g) was found by adding the optimization energy (E_{opt}) and the thermal correction factor ($E_{Thermal}$), according to Equation (1).

$$E_g = E_{opt} + E_{Thermal} \quad (1)$$

The energy of the solvated molecule (E_{solv}) was determined by performing an energy calculation by solvating the optimized structure in N,N-dimethylformamide (DMF) using the default solvent model in Gaussian 09, the integral equation formalism variant of the polarizable continuum model (IEFPCM). Then, the difference between the energy of the solvated molecule (E_{solv}) and the energy of the gas-phase molecule (E_g) was used to calculate the change in Gibbs free energy of solvation (ΔG_{solv}), according to Equation (2).

$$\Delta G_{solv} = E_{solv} - E_g \quad (2)$$

The change in Gibbs free energy associated with the reduction is found by subtracting the E_g from the structures varying by one electron. For example, Equation (3) demonstrates that the change in Gibbs free energy for wave 1 ($\Delta G_{red,wave1(g)}$) is found by subtracting the energy of the neutral structure ($E_{g,n}$) from the energy of the anion product ($E_{g,a}$).

$$\Delta G_{red,\ wave1(g)} = E_{g,a} - E_{g,n} \quad (3)$$

Figure 4 shows the visual representation of the thermodynamic cycles used to calculate the change in Gibbs free energies for the reduction in solvent. Figure 4a shows the thermodynamic cycles associated with the first (wave 1) and second (wave 2) reduction of the diazine ring for the non-nitro group containing derivatives (derivatives A1-D4), $\Delta G_{red,wave1(solv)}$, and $\Delta G_{red,wave2(solv)}$, respectively. Figure 4b shows the modified thermodynamic cycles used to calculate the first reduction of the diazine ring (wave 1), the reduction of the nitro group (nitro wave), and the second reduction of the diazine ring (wave 2) for the derivatives containing a nitro group (derivatives E1-E4).

For example, wave 1 is calculated according to Equation (4),

$$\Delta G_{red,\ wave1(solv)} = -\Delta G_{solv,n} + \Delta G_{red,wave1(g)} + \Delta G_{solv,a} \quad (4)$$

where $\Delta G_{solv,n}$ is the neutral molecule change in Gibbs free energy of solvation, $\Delta G_{red,wave1(g)}$ is the change in Gibbs free energy of the reduction in the gas phase and $\Delta G_{solv,a}$ is the radical anion change in Gibbs free energy of solvation.

The ΔG_{red} values were used to calculate the reduction potentials for comparison to the experimental data. The following equation shows the calculation of the reduction potential for wave 1 ($\varepsilon_{red,wave1}$) from the $\Delta G_{red,wave1}$, where F is Faraday's constant (96,485 C/mole) and n is the number of electrons per reduction.

$$\varepsilon_{red,wave1} = \frac{-\Delta G_{red,wave1(solv)}}{nF} \quad (5)$$

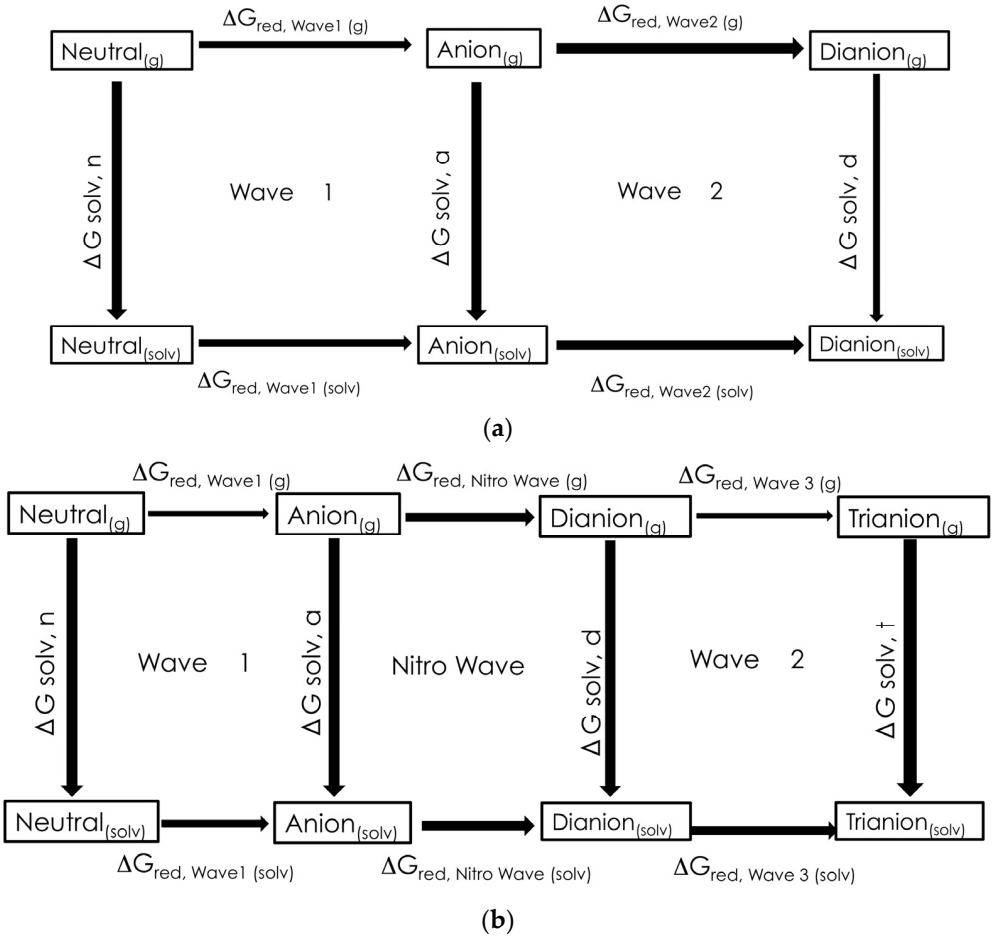

Figure 4. Visual representation of the thermodynamic cycles used to calculate the change in free energy of reduction (ΔG_{red}): (**a**) wave 1 (first reduction of the diazine ring) and wave 2 (second reduction of the diazine ring) for derivatives without a nitro group (A1-D4) and (**b**) wave 1 (first reduction of the diazine ring), nitro wave (nitro group reduction) and wave 2 (second reduction of the diazine ring) for derivatives containing a nitro group (E1-E4).

2.3. Ferrocene/Ferrocenium Reference

The structures of ferrocene (*Fc*) and ferrocenium ion (Fc^+) were constructed in Gaussian View 5 [35] and the DFT calculations were carried out in Gaussian 09 [36], as described above for the quinoxaline derivatives. The B3LYP/cc-pVTZ predicted reduction potential for the Fc/Fc^+ reaction ($\varepsilon_{Fc/Fc+}$) was used as the reference for the calculated reduction potentials according to Equation (6), since the experimental redox potentials were measured with reference to a Fc/Fc^+ electrode ion [31].

$$\varepsilon_{cell} = \varepsilon_{red,wave1} - \varepsilon_{Fc/Fc+} \quad (6)$$

Lastly, the adjusted reduction cell potential was found by adjusting the potential of the Fc/Fc^+ half-cell potential to zero according to Equation (7), since the Fc/Fc^+ electrode in the experiment was set to zero.

$$\varepsilon'_{cell} = \varepsilon_{cell} + 0.72 \text{ V} \quad (7)$$

3. Results and Discussion

3.1. Computationally Predicted Electrochemical Reduction Potentials

The B3LYP/cc-pVTZ predicted half-cell potential for the Fc/Fc^+ half-cell was found to be 5.17 V. The calculated B3LYP/cc-pVTZ reduction potentials for the 20 quinoxaline 1,4-di-N-oxide derivatives are tabulated in Table 2 and are listed beside the previously

calculated half-cells with the lanl2dz and 6-31G basis sets. Computational log files are in Supplemental Materials (S1). All 20 derivatives were well-behaved with the cc-pVTZ basis set with their optimized structures looking as expected and their calculated potentials falling within the expected range. The carbon–chloride bond length lengthened in the optimization calculation for trianion structure E4 with the lanl2dz and 6-31G basis set. The cc-pVTZ basis set had a reasonable carbon–chloride bond length of 1.78 Å. The cc-pVTZ is a more robust basis set which includes polarization d and f functions. It was expected that the cc-pVTZ basis set would do a better job of predicting the optimized structures, especially for the anion species. The adjusted electrochemical cell potentials versus the Fc/Fc^+ half-cell with Fc/Fc^+ set to zero are shown in Table 3 and are listed beside the previously calculated adjusted cell potentials for the lanl2dz and 6-31G basis sets.

Table 2. Wave 1, nitro wave, and wave 2 half-cell reaction potentials (in volts) calculated using B3LYP/cc-pVTZ and the previously calculated B3LYP/lanl2dz and B3LYP/6-31G predictions [27].

	Wave 1			Nitro Wave			Wave 2		
Compound	**cc-pVTZ**	**lanl2dz**	**6-31G**	**cc-pVTZ**	**lanl2dz**	**6-31G**	**cc-pVTZ**	**lanl2dz**	**6-31G**
A1	3.37	3.60	3.29	—	—	—	2.08	2.18	1.78
A2	3.31	3.55	3.24	—	—	—	2.07	2.16	1.77
A3	3.33	3.58	3.27	—	—	—	2.11	2.23	1.83
A4	3.49	3.75	3.46	—	—	—	2.26	2.40	2.02
B1	3.36	3.59	3.28	—	—	—	2.06	2.16	1.76
B2	3.30	3.54	3.23	—	—	—	2.05	2.09	1.75
B3	3.32	3.57	3.26	—	—	—	2.10	2.22	1.82
B4	3.47	3.74	3.45	—	—	—	2.25	2.39	1.79
C1	3.40	3.65	3.35	—	—	—	2.10	2.19	1.81
C2	3.37	3.61	3.31	—	—	—	2.09	2.12	1.81
C3	3.37	3.63	3.33	—	—	—	2.13	2.25	1.86
C4	3.52	3.80	3.52	—	—	—	2.27	2.41	2.04
D1	3.40	3.64	3.33	—	—	—	2.10	2.19	1.81
D2	3.34	3.58	3.28	—	—	—	2.09	2.12	1.80
D3	3.36	3.62	3.31	—	—	—	2.13	2.24	1.86
D4	3.52	3.78	3.50	—	—	—	2.27	2.40	2.04
E1	3.48	8.05	7.77	2.47	−4.22	−4.72	2.43	5.62	5.41
E2	3.43	8.00	7.72	2.48	−4.18	−4.63	2.44	5.58	5.26
E3	3.42	7.96	7.67	2.54	−4.09	−4.53	2.50	5.58	5.22
E4	3.57	7.98	7.65	2.76	−3.88	No Value *	2.58	5.72	No Value *

* Trianion structure had optimization issues so no electrochemical potential could be determined.

Table 3. The adjusted electrochemical wave 1, nitro wave, and wave 2 reaction potentials (ε'_{cell}, in Volts) with the Fc/Fc^+ reduction potential set to zero calculated using B3LYP/cc-pVTZ and the previously calculated B3LYP/lanl2dz and B3LYP/6-31G predictions [27].

	Wave 1			Nitro Wave			Wave 2		
Compound	**cc-pVTZ**	**lanl2dz**	**6-31G**	**cc-pVTZ**	**lanl2dz**	**6-31G**	**cc-pVTZ**	**lanl2dz**	**6-31G**
A1	−1.09	−1.19	−1.17	—	—	—	−2.37	−2.62	−2. 69
A2	−1.10	−1.25	−1.22	—	—	—	−2.39	−2.63	−2.69
A3	−1.05	−1.21	−1.19	—	—	—	−2.35	−2.56	−2.63
A4	−1.06	−1.05	−1.00	—	—	—	−2.35	−2.40	−2.44
B1	−1.14	−1.20	−1.18	—	—	—	−2.38	−2.63	−2.70
B2	−1.15	−1.26	−1.23	—	—	—	−2.40	−2.71	−2.71
B3	−1.08	−1.22	−1.20	—	—	—	−2.36	−2.58	−264
B4	−1.11	−1.06	−1.01	—	—	—	−2.36	−2.40	−2.69
C1	−1.12	−1.14	−1.11	—	—	—	−2.34	−2.60	−2.65
C2	−1.13	−1.18	−1.15	—	—	—	−2.35	−2.68	−2.65
C3	−1.09	−1.16	−1.13	—	—	—	−2.32	−2.55	−2.60
C4	−1.10	−1.00	−0.94	—	—	—	−2.32	−2.39	−2.42

Table 3. *Cont.*

	Wave 1			Nitro Wave			Wave 2		
Compound	**cc-pVTZ**	**lanl2dz**	**6-31G**	**cc-pVTZ**	**lanl2dz**	**6-31G**	**cc-pVTZ**	**lanl2dz**	**6-31G**
D1	−0.97	−1.16	−1.13	—	—	—	−2.19	−2.60	−2.65
D2	−0.98	−1.21	−1.18	—	—	—	−2.20	−2.67	−2.66
D3	−0.93	−1.18	−1.15	—	—	—	−2.18	−2.55	−2.60
D4	−0.94	−1.01	−0.96	—	—	—	−2.18	−2.39	−2.42
E1	−0.97	3.26	3.31	−1.98	−9.01	−1.15	−2.02	0.82	0.95
E2	−1.03	3.21	3.26	−1.98	−8.98	−1.20	−2.02	0.78	0.80
E3	−1.03	3.17	3.21	−1.91	−8.88	−1.25	−1.95	0.79	0.76
E4	−0.88	3.18	3.19	−1.69	−8.67	No Value *	−1.88	0.93	No Value *

* Trianion structure had optimization issues so not electrochemical potential could be determined.

3.2. Comparison to Experimental Electrochemical Data

Table 4 shows the referenced experimental electrochemical reduction data for wave 1, the nitro wave, and wave 2 [33]. All experimental electrochemical reduction potentials were reported compared to the Fc/Fc^+ electrode. Wave 1 is reversible in the experimental data set for all compounds except derivative C3. In the experimental data set, the electrochemical reduction potential for derivative C3 is determined from only the cathodic potential. For the other 19 derivatives, the difference between $E_{1/2}$ (average of the cathodic and anodic peaks) and E_{pc} (cathodic peak only) ranges from 0.035 to 0.65 V; therefore, it would be expected for the irreversibility to make C3 an experimental outlier [33]. Moreover, C3 has no reported wave 2 value. For these reasons, C3 is not considered in the analysis of the computational data sets. Additionally, the B1 and D1 derivatives are noted as having a shoulder in their wave 2 voltammograms [33]. Despite this potential concern about the experimental data, we opted to include B1 and D1 in the data analysis for wave 2.

Table 4. The experimental electrochemical wave 1, nitro wave, and wave 2 reduction potentials (ε'_{cell}, in volts) measured versus the Fc/Fc^+ electrode. [33].

Compound	**Wave 1 $E_{1/2}$ (V)**	**Nitro Wave $E_{1/2}$ (V)**	**Wave 2 E_{pc}(V)**
A1	−1.296	—	−2.163
A2	−1.327	—	−2.310
A3	−1.331	—	−2.166
A4	−1.188	—	−1.973
B1	−1.309	—	−2.56 [b]
B2	−1.318	—	−2.377
B3	−1.333	—	−2.216
B4	−1.196	—	−2.115
C1	−1.269	—	−2.097
C2	−1.303	—	−2.125
C3	−1.401 [a]	—	No Value
C4	−1.154	—	−2.080
D1	−1.278	—	−2.06 [b]
D2	−1.305	—	−2.326
D3	−1.300	—	−1.995
D4	−1.181	—	−2.132
E1	−1.234	−1.518	−2.306
E2	−1.265	−1.539	−2.352
E3	−1.277	−1.566	−2.372
E4	−1.134	−1.514	−2.141

a. Irreversible b. Shoulder [33].

3.2.1. Comparison of Predicted and Experimental Wave 1 Electrochemical Potentials

The correlation between the predicted and experimental values of wave 1 for the B3LYP/cc-pVTZ, B3LYP/lanl2dz, and B3LYP/6-31G methods are shown in Figure 5. Figure 5a excludes C3 and Figure 5b excludes C3 and the nitro group containing derivatives E1-E4. Figure 5a demonstrates that the B3LYP/cc-pVTZ does the best job at predicting the electrochemical potentials. The best fit for the B3LYP/cc-pVTZ data is y = 1.24x + 0.52 with R^2 of 0.949 and a standard error of the y-estimate (hereafter, standard error) is 0.019 V, while the best-fit for the B3LYP/lanl2dz and B3LYP/6-31G methods are y = 9.70x + 12.02 with R^2 of 0.111 and standard error of 1.8 V and y = 9.76x + 12.12 with R^2 of 0.113 and standard error of 1.8 V, respectively.

The nitro group containing derivatives were clear outliers in the B3LYP/lanl2dz and B3LYP/6-31G data. Once the nitro group containing compounds are removed from consideration (Figure 5b), the ability for the B3LYP/lanl2dz and B3LYP/6-31G methods to calculate wave 1 improves dramatically. Without the nitro groups containing compounds, the best-fit for the B3LYP/lanl2dz, and B3LYP/6-31G methods are y = 1.38x + 0.6 with R^2 of 0.963 and standard error of 0.018 V and y = 1.52x + 0.81 with R^2 of 0.968 and standard error of 0.018 V, respectively. The best-fit for the B3LYP/cc-pVTZ for wave 1 without the nitro groups appears to improve slightly to y = 1.20x + 0.46 with R^2 of 0.969 and standard error of 0.014 V. However, the slope and intercept do not vary by more than their relative uncertainties. Without the nitro group containing derivatives, all the methods had strong correlations, with $R^2 > 0.96$ and similar standard errors.

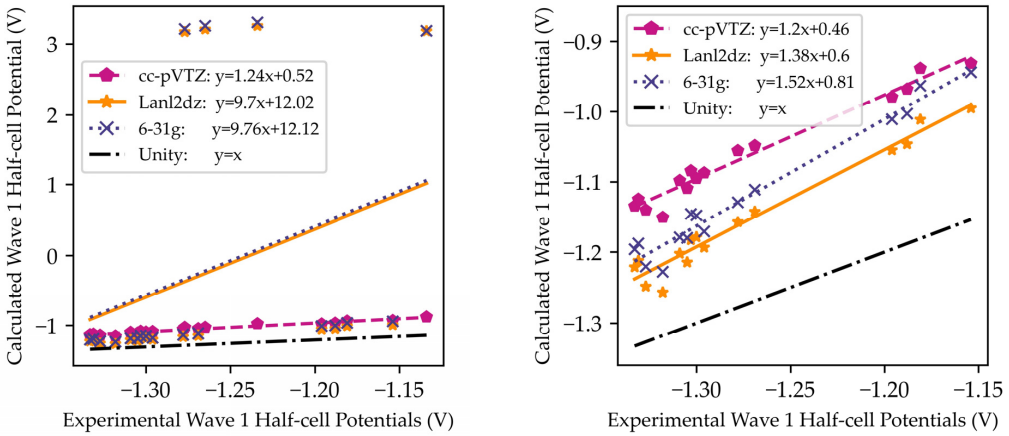

(**a**) (**b**)

Figure 5. Comparison of computational electrochemical cell potentials vs. experimental [31] electrochemical cell potentials for (**a**) wave 1 and (**b**) wave 1 with the nitro group containing derivatives (E1-E4) removed from analysis. The B3LYP/cc-pVTZ method is indicated by pink pentagons and the previously calculated methods B3LYP/lanl2dz and B3LYP/6-31G [27] are indicated with blue crosses and yellow stars, respectively. Derivative C3 is excluded from analysis.

3.2.2. Comparison of Predicted and Experimental Wave 2 Electrochemical Potentials

Figure 6 shows the correlation between predicted and experimental values of wave 2 for the B3LYP/cc-pVTZ, B3LYP/lanl2dz, and B3LYP/6-31G methods. Figure 6a excludes C3. The best fit for the B3LYP/cc-pVTZ, B3LYP/lanl2dz, and B3LYP/6-31G methods are y = −0.012x − 2.27 with R^2 of 0.00013 and standard error of 0.17 V, y = −2.54x − 7.44 with R^2 of 0.0732 and standard error of 1.4 V, and y = −3.13x − 8.94 with R^2 of 0.134 and standard error of 1.3 V, respectively. The predicted electrochemical potentials using the B3LYP/cc-pVTZ, B3LYP/lanl2dz, and B3LYP/6-31G methods show no correlation with the experimental results. The Appendix A Figure A2a shows the correlation between the predicted and the experimental values for wave 2 excluding B1, C3, and D1. The correlation

improves slightly with the removal of the B1 and D1 derivatives (shoulder in experimental data). The best fit for the B3LYP/cc-pVTZ, B3LYP/lanl2dz, and B3LYP/6-31G methods are y = −0.17x − 2.61 with an R^2 of 0.0175 and standard error of 0.17 V, y = −4.71x − 12.07 with a R^2 of 0.1663 and standard error of 1.4 V, and y = −5.52x − 14.07 with an R^2 of 0.2739 and standard error of 1.2 V, respectively.

Figure 6b demonstrates that even with the nitro group containing compounds removed, there is a low correlation with the experimental data. The best fit for the B3LYP/cc-pVTZ, B3LYP/lanl2dz, and B3LYP/6-31G methods are y = 0.30x − 1.66 with R^2 of 0.327 and standard error of 0.07 V, y = 0.40x − 1.68 with R^2 of 0.313 and standard error of 0.097 V, and y = 0.36x − 1.83 with R^2 of 0.307 and standard error of 0.088 V, respectively. Like the wave 1 results, once the nitro group containing derivatives are removed, all three methods improved their predictive ability and have a similar correlation with the experimental data with R^2 ranging from 0.307 to 0.327. It is worth noting that the removal of derivatives B1 and D1, which were indicated in the experimental data set as having a shoulder, does improve the correlation to experiment for the non-nitro-group containing derivatives (Appendix A Figure A2b). The best fits for the B3LYP/cc-pVTZ, B3LYP/lanl2dz, and B3LYP/6-31G methods improve to y = 0.43x − 1.37 with R^2 of 0.379 and standard error of 0.07 V, y = 0.64x − 1.17 with R^2 of 0.430 and standard error of 0.094 V, and y = 0.52x − 1.47 with R^2 of 0.360 and standard error of 0.089 V, respectively. The elimination of B1 and D1 from the comparison does increase the correlation of the data with R^2 values now between 0.360 and 0.430; and, unexpectedly, the lanl2dz basis set has the best correlation when B1 and D1 are removed from analysis.

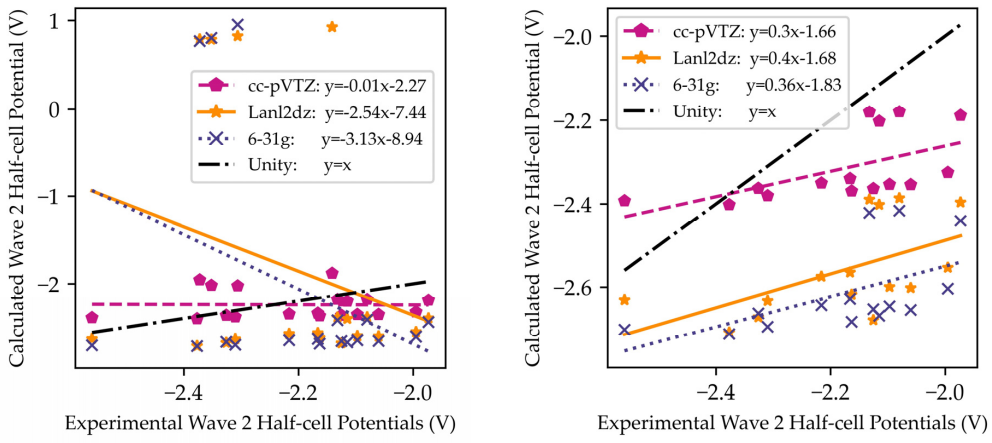

(**a**) (**b**)

Figure 6. Comparison of computational electrochemical cell potentials vs. experimental [31] electrochemical cell potentials for (**a**) wave 2 and (**b**) wave 2 with the nitro group containing derivatives (E1-E4) removed from analysis. The B3LYP/cc-pVTZ method is indicated by pink pentagons and the previously calculated methods B3LYP/lanl2dz and B3LYP/6-31G [27] are indicated with blue crosses and yellow stars, respectively. Derivative C3 is excluded from analysis.

3.2.3. Comparison of the Predicted and Experimental Nitro-Wave Electrochemical Potentials

Figure 7 shows the correlation of the experimental and predicted nitro-wave for the nitro-group containing compounds E1-E4 for the B3LYP/cc-pVTZ, B3LYP/lanl2dz, and B3LYP/6-31G methods. All three methods do a poor job of calculating the nitro wave. The best fits for the B3LYP/cc-pVTZ, B3LYP/lanl2dz, and B3LYP/6-31G methods are y = 2.12x + 1.36 with R2 of 0.138 and standard error of 0.15 V, y = 1.51x − 6.56 with R2 of 0.057 and standard error of 0.057 V, and y = −3.94x + 15.17 with R2 of 0.997 and standard error of 0.0068 V, respectively. The R^2 value of the B3LYP/6-31G method is artificially high as the comparison only included E1-E3 due to the method's inability to optimize the trianion structure of E4. With only three data points, the artificially high R^2 value should not be considered

an indication of good correlation of the predicted electrochemical potentials with the experimental potentials. The inability for all three methods to adequately predict the nitro wave may indicate that none of the methods are correctly determining the dianion structure for the nitro group containing compounds.

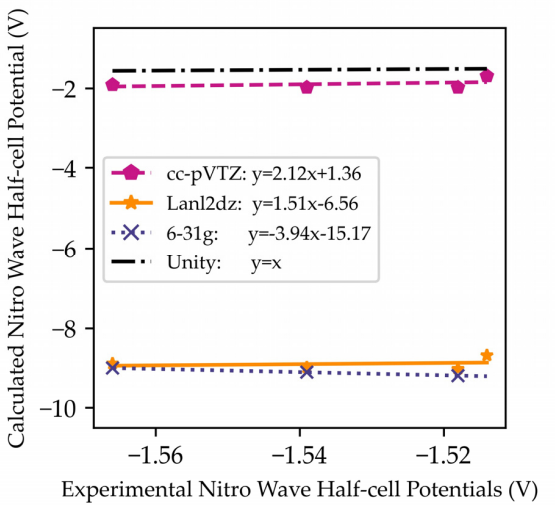

Figure 7. Comparison of computational electrochemical cell potentials vs. experimental [33] electrochemical cell potentials for the nitro wave for the nitro group containing derivatives (E1-E4). The B3LYP/cc-pVTZ method is indicated by pink pentagons and the previously calculated methods B3LYP/lanl2dz and B3LYP/6-31G [27] are indicated with blue crosses and yellow stars, respectively.

4. Conclusions

The ability of the B3LYP/cc-pVTZ method to calculate experimental electrochemical potentials for a series of 20 quinoxaline 1,4-di-N-oxide derivatives was investigated and compared to the previous results for B3LYP/lanl2dz and B3LYP/6-31G methods. The B3LYP/cc-pVTZ method had increased ability to calculate the first reduction potential of the diazine ring (wave 1) as the cc-pVTZ basis set was able to calculate the wave 1 reduction potentials for the nitro-group containing derivatives. However, when the nitro groups containing derivatives were removed, the correlation between the B3LYP/cc-pVTZ method and experiment is very similar to the correlations to the B3LYP/lanl2dz and B3LYP/6-31G methods and experiment.

The cc-pVTZ basis set did not provide a major improvement for calculating second reduction potentials for the diazine ring (wave 2). The correlation between the B3LYP/cc-pVTZ predicted wave 2 electrochemical potentials and the experimental data was very weak. When the nitro group containing derivatives (E1-E4) and the experimental outliers (B1 and D1) were excluded, the lanl2dz basis set had the most correlation with the experimental data based upon the R^2 values. None of the methods were able to correctly predict the electrochemical potentials for the reduction of the nitro group in the nitro group containing derivatives. The B3LYP/cc-pVTZ method was able to optimize the dianion and trianion nitro group containing derivatives successfully, which was an improvement to the artificial C–Cl bond lengthening previously observed in E4 with the B3LYP/lanl2dz and B3LYP/6-31G methods.

While all three methods provide a strong correlation to experimental data for wave 1, we were surprised that the B3LYP/cc-pVTZ method poorly predicted the reduction potentials for wave 2 and the nitro wave. We had expected to have improved correlation to wave 2 with the cc-pVTZ predictions. The inability of B3LYP/lanl2dz to predict wave 2, while giving a strong correlation between predicted and experimental wave 1 potentials is also observed in the set of 37 1,4-di-N-oxide quinoxaline-2-carboxamide derivatives (unpublished) [31]. Considering combined data of all three of our reduction potential prediction studies, we hypothesize that the system may be undergoing structural changes with the addition of the second electron to the system and that the chemistry may not be

as straightforward as the scheme shown in Figure 1. Given the reactivity of the chemical species created during the addition of the electrons, it is possible that the derivatives may be interacting with solvent, electrolytes, or other quinoxaline molecules present in the solution. Unfortunately, structural changes during reduction were not investigated during the experimental study.

Supplementary Materials: The following supporting information can be downloaded at: https://www.mdpi.com/article/10.3390/computation11010009/s1, computational log files.

Author Contributions: Conceptualization, P.W.C. and C.M.R.; methodology, C.M.R.; software, S.B., P.M., J.M.K. and C.M.R.; data curation, S.B., P.M., J.M.K. and C.M.R.; validation, S.B. and P.M.; formal analysis, S.B., P.M., J.M.K. and C.M.R.; investigation, S.B. and P.M.; resources, P.W.C., J.M.K. and C.M.R.; writing—original draft preparation, S.B., P.M., P.W.C., J.M.K. and C.M.R.; writing—review and editing, S.B., P.M., P.W.C., J.M.K. and C.M.R.; visualization, J.M.K. and C.M.R.; supervision, P.W.C. and C.M.R.; project administration, C.M.R. All authors have read and agreed to the published version of the manuscript.

Funding: This research received no external funding.

Data Availability Statement: The computational log files created in this study can be located in Supplemental Materials (S1).

Acknowledgments: Some of the computation for this work was performed on the high-performance computing infrastructure provided by Research Support Solutions and in part by the National Science Foundation under grant number CNS-1429294 at the University of Missouri, Columbia MO. DOI: https://doi.org/10.32469/10355/69802 (accessed on 1 December 2022).

Conflicts of Interest: The authors declare no conflict of interest.

Appendix A

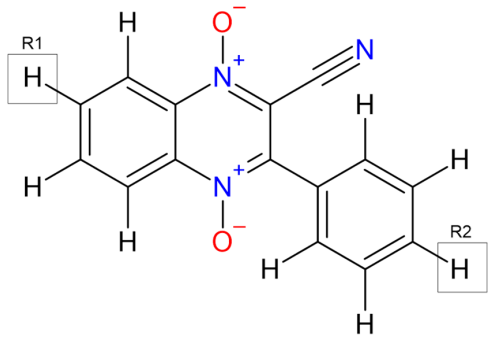

Derivative A1

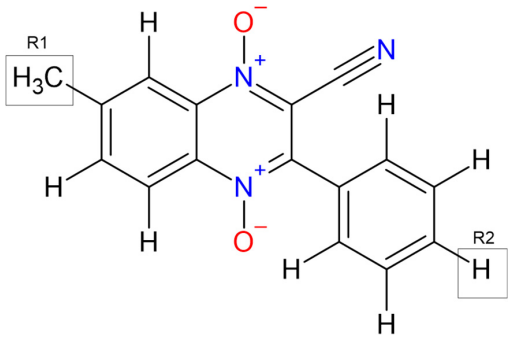

Derivative A2

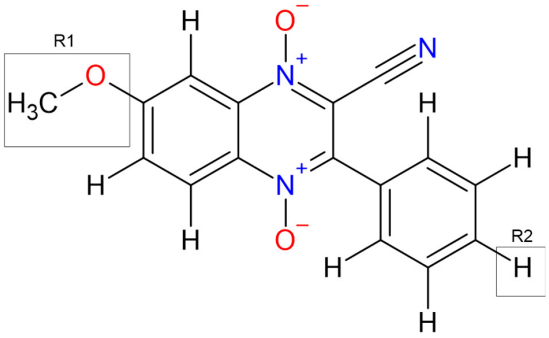

Derivative A3

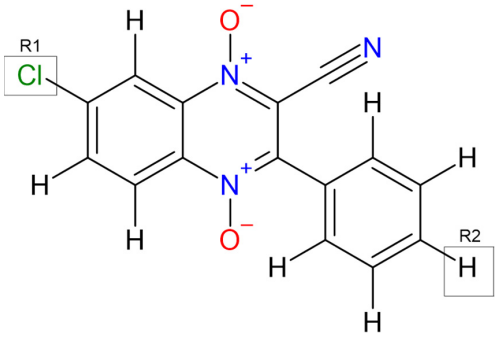

Derivative A4

Figure A1. *Cont.*

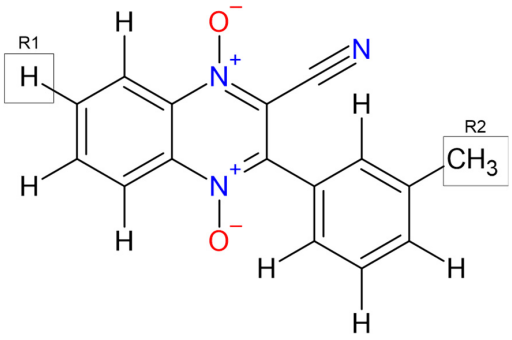

Derivative B1

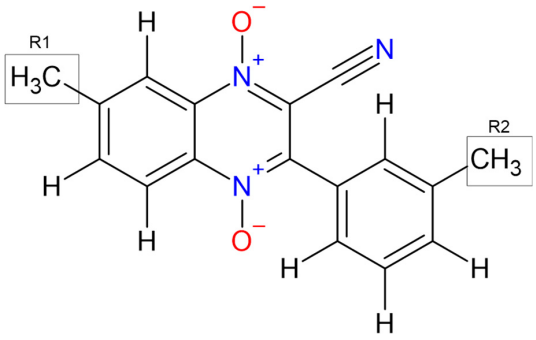

Derivative B2

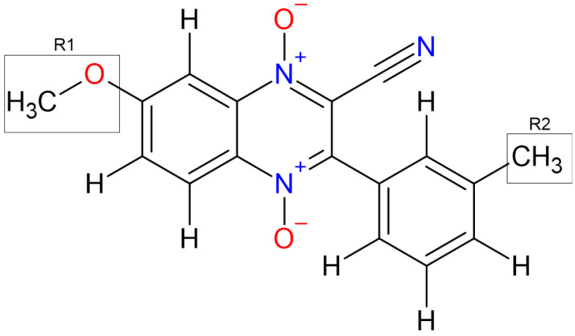

Derivative B3

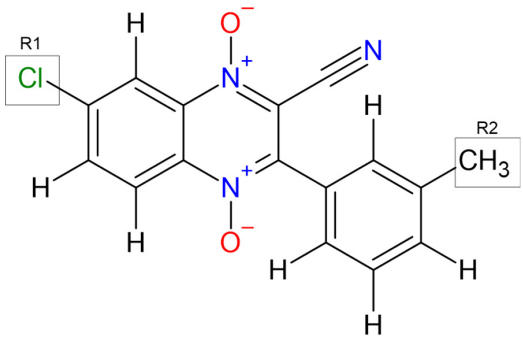

Derivative B4

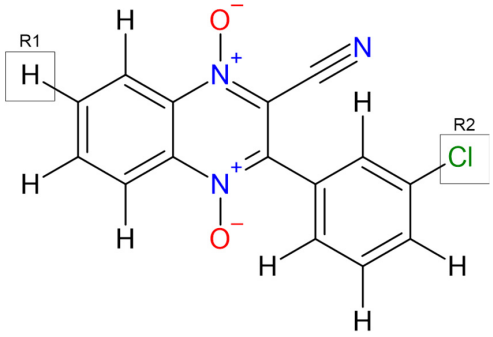

Derivative C1

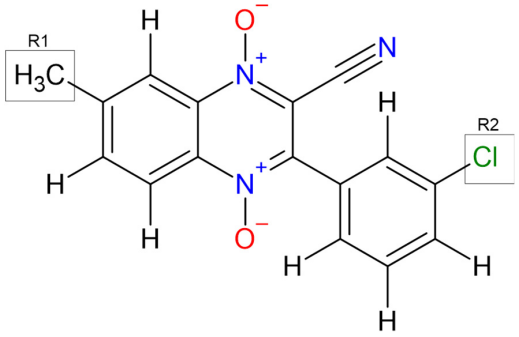

Derivative C2

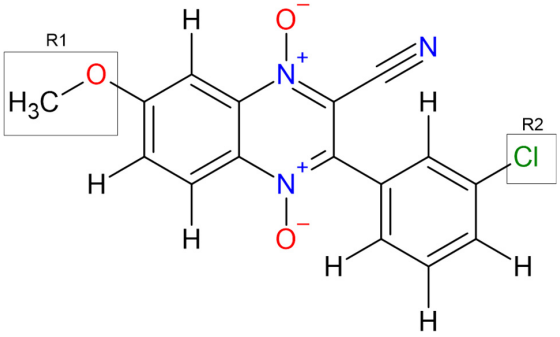

Derivative C3

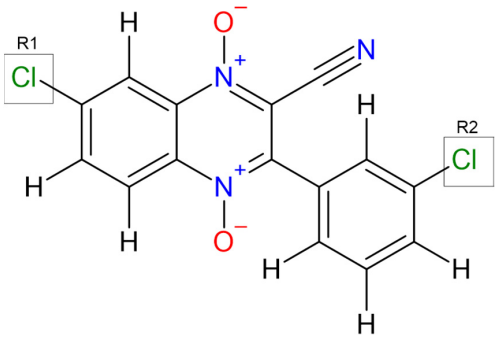

Derivative C4

Figure A1. *Cont.*

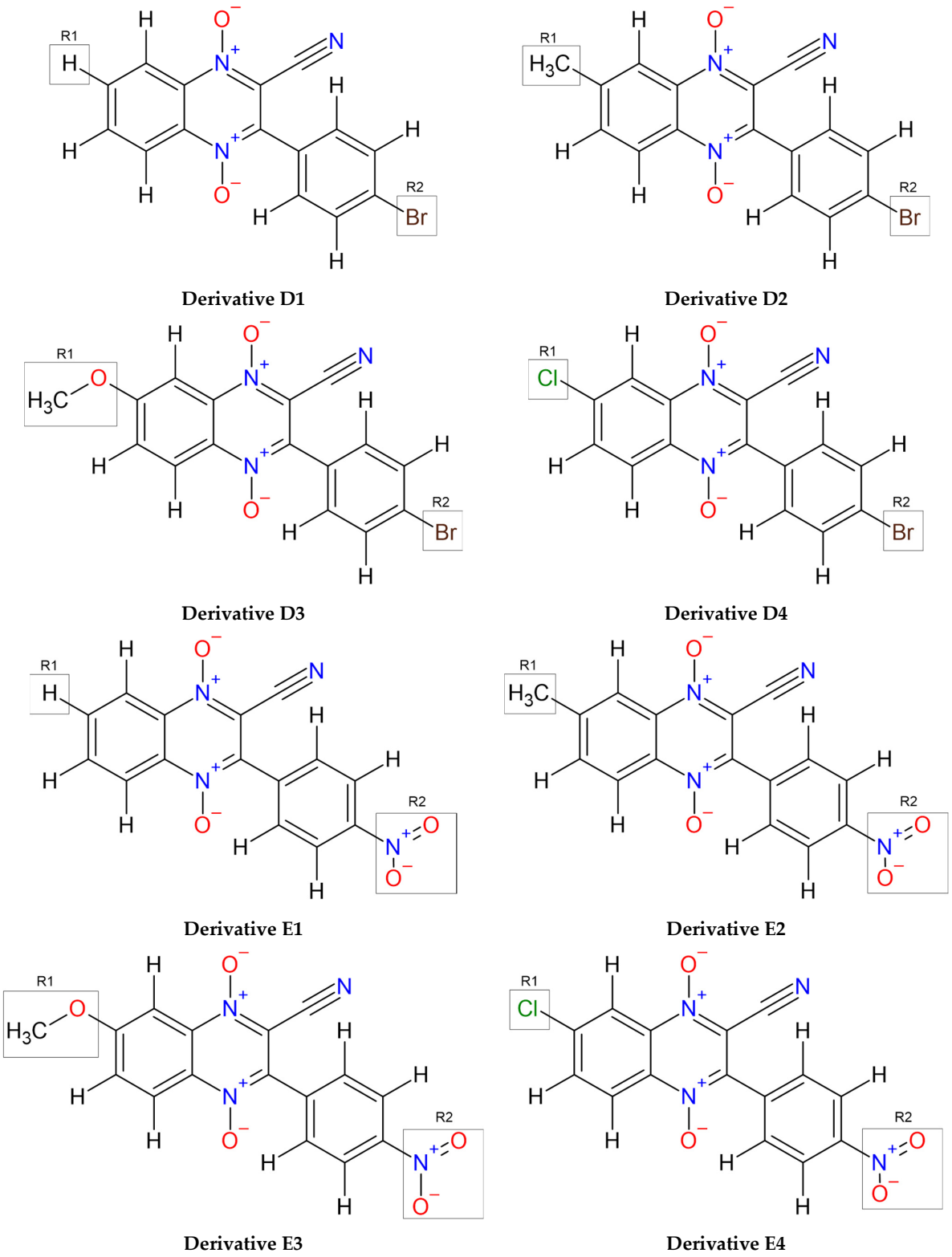

Figure A1. Structures of the 3-Aryl-Quinoxaline-2-Carbonitrile 1,4-Di-N-Oxide derivatives drawn with ChemSketch Freeware [19]. The substituent R1 and R2 groups are labeled.

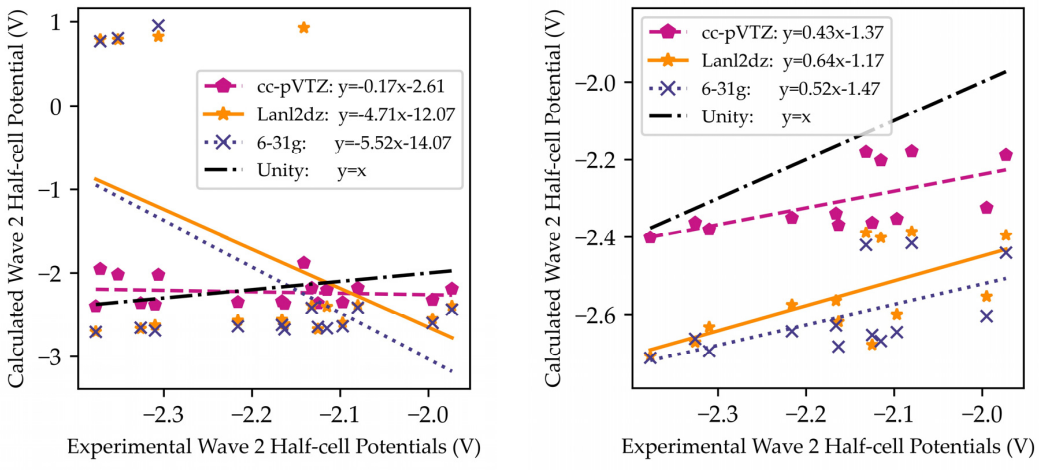

(**a**) (**b**)

Figure A2. Comparison of computational electrochemical cell potentials vs. experimental electrochemical cell potentials for (**a**) wave 2 and (**b**) wave 2 without the nitro groups. The B3LYP/cc-pVTZ method is indicated by pink pentagons and the previously calculated methods B3LYP/lanl2dz and B3LYP/6-31G [27] are indicated with blue crosses and yellow stars, respectively. Derivative C3, B1 and D1are excluded from analysis.

References

1. Anderson, R.F.; Yadav, P.; Shinde, S.S.; Hong, C.R.; Pullen, S.M.; Reynisson, J.; Wilson, W.R.; Hay, M.P. Radical chemistry and cytotoxicity of bioreductive 3-substituted quinoxaline di-N-Oxides. *Chem. Res. Toxicol.* **2016**, *29*, 1310–1324. [CrossRef] [PubMed]
2. Zarranz, B.; Jaso, A.; Aldana, I.; Monge, A. Synthesis and anticancer activity evaluation of new 2-alkylcarbonyl and 2-benzoyl-3-trifluoromethyl-quinoxaline 1,4-di-N-oxide derivatives. *Bioorg. Med. Chem.* **2004**, *12*, 3711–3721. [CrossRef] [PubMed]
3. Amin, K.M.; Ismail, M.M.F.; Noaman, E.; Soliman, D.H.; Ammar, Y.A. New quinoxaline 1,4-di-N-oxides. Part 1: Hypoxia-selective cytotoxins and anticancer agents derived from quinoxaline 1,4-di-N-oxides. *Bioorg. Med. Chem.* **2006**, *14*, 6917–6923. [CrossRef] [PubMed]
4. Suter, W.; Rosselet, A.; Knusel, F. Mode of action of quindoxin and substituted quinoxaline-di-N-oxides on Escherichia coli. *Antimicrob. Agents Chemother.* **1978**, *13*, 770–783. [CrossRef]
5. Soliman, D.H. Anti-bacterial and Anti-fungal Activities of New Quinoxaline 1,4-di-N-Oxide Derivatives. *Int. J. Org. Chem.* **2013**, *3*, 65–72. [CrossRef]
6. Vicente, E.; Pérez-Silanes, S.; Lima, L.M.; Ancizu, S.; Burguete, A.; Solano, B.; Villar, R.; Aldana, I.; Monge, A. Selective activity against Mycobacterium tuberculosis of new quinoxaline 1,4-di-N-oxides. *Bioorg. Med. Chem.* **2009**, *17*, 385–389. [CrossRef]
7. Estevez, Y.; Quiliano, M.; Burguete, A.; Cabanillas, B.; Zimic, M.; Málaga, E.; Verástegui, M.; Pérez-Silanes, S.; Aldana, I.; Monge, A.; et al. Trypanocidal properties, structure–activity relationship and computational studies of quinoxaline 1,4-di-N-oxide derivatives. *Exp. Parasitol.* **2011**, *127*, 745–751. [CrossRef]
8. Ancizu, S.; Moreno, E.; Torres, E.; Burguete, A.; Pérez-Silanes, S.; Benítez, D.; Villar, R.; Solano, B.; Marín, A.; Aldana, I.; et al. Heterocyclic-2-carboxylic Acid (3-Cyano-1,4-di-N-oxidequinoxalin-2-yl)amide Derivatives as Hits for the Development of Neglected Disease Drugs. *Molecules* **2009**, *14*, 2256–2272. [CrossRef] [PubMed]
9. Torres, E.; Moreno-Viguri, E.; Galiano, S.; Devarapally, G.; Crawford, P.W.; Azqueta, A.; Arbillaga, L.; Varela, J.; Birriel, E.; Di Maio, R.; et al. Novel quinoxaline 1,4-di-N-oxide derivatives as new potential antichagasic agents. *Eur. J. Med. Chem.* **2013**, *66*, 324–334. [CrossRef]
10. Zarranz, B.; Jaso, A.; Aldana, I.; Monge, A.; Maurel, S.; Deharo, E.; Jullian, V.; Sauvain, M. Synthesis and antimalarial activity of new 3-arylquinoxaline-2-carbonitrile derivatives. *Arzneimittelforschung* **2005**, *55*, 754–761.
11. Carta, A.; Paglietti, G.; Rahbar Nikookar, M.E.; Sanna, P.; Sechi, L.; Zanetti, S. Novel substituted quinoxaline 1,4-dioxides with in vitro antimycobacterial and anticandida activity. *Eur. J. Med. Chem.* **2002**, *37*, 355–366. [CrossRef] [PubMed]
12. Burguete, A.; Pontiki, E.; Hadjipavlou-Litina, D.; Ancizu, S.; Villar, R.; Solano, B.; Moreno, E.; Torres, E.; Pérez, S.; Aldana, I. Synthesis and biological evaluation of new quinoxaline derivatives as antioxidant and anti-inflammatory agents. *Chem. Biol. Drug Des.* **2011**, *77*, 255–267. [CrossRef] [PubMed]
13. Burguete, A.; Pontiki, E.; Hadjipavlou-Litina, D.; Villar, R.; Vicente, E.; Solano, B.; Ancizua, S.; Pérez-Silanesa, S.; Aldanaa, I.; Mongea, A. Synthesis and anti-inflammatory/antioxidant activities of some new ring substituted 3-phenyl-1-(1,4-di-N-oxide quinoxalin-2-yl)-2-propen-1-one derivatives and of their 4,5-dihydro-(1H)-pyrazole analogues. *Bioorg. Med. Chem. Lett.* **2007**, *17*, 6439–6443. [CrossRef] [PubMed]

14. Gonzalez, M.; Cerecetto, H.; Monge, A. Quinoxaline 1,4-dioxide and phenazine 5,10-dioxide chemistry and biology. *Top. Heterocycl. Chem.* **2007**, *11*, 179–211.
15. Crawford, P.W.; Scamehorn, R.G.; Hollstein, U.; Ryan, M.D.; Kovacic, P. Cyclic voltammetry of phenazines and quinoxalines including mono-and di-N-oxides. Related to structure and antimicrobial activity. *Chem. Biol. Interact.* **1986**, *60*, 67–84. [CrossRef]
16. Moreno, E.; Pérez-Silanes, S.; Gouravaram, S.; Macharam, A.; Ancizu, S.; Torres, E.; Aldana, I.; Monge, A.; Crawford, P.W. 1,4-Di-N-oxide quinoxaline-2-carboxamide: Cyclic voltammetry and relationship between electrochemical behavior, structure and anti-tuberculosis activity. *Electrochim. Acta* **2011**, *56*, 3270–3275. [CrossRef]
17. Carta, A.; Corona, P.; Loriga, M. Quinoxaline 1,4-dioxide: A versatile scaffold endowed with manifold activities. *Curr. Med. Chem.* **2005**, *12*, 2259–2272. [CrossRef]
18. Cheng, G.; Sa, W.; Cao, C.; Guo, L.; Hao, H.; Liu, Z.; Wang, X.; Yuan, Z. Quinoxaline 1,4-di-N-oxides: Biological activities and mechanisms of action. *Front. Pharmacol.* **2016**, *7*, 64. [CrossRef]
19. *ACD/ChemSketch, Version 2022.1.0*; Advanced Chemistry Development, Inc. (ACD/Labs): Toronto, ON, Canada, 2022. Available online: https://www.acdlabs.com (accessed on 26 December 2022).
20. Divya, K.M.; Savitha, D.P.; Anjali Krishna, G.; Dhanya, T.M.; Mohanan, P.V. Crystal structure, DFT studies, Hirshfeld surface and energy framework analysis of 4-(5-nitro-thiophen-2-yl)-pyrrolo [1, 2-a] quinoxaline: A potential SARS-CoV-2 main protease inhibitor. *J. Mol. Structure.* **2022**, *1251*, 131932. [CrossRef]
21. Verbitskiy, E.V.; le Poul, P.; Bureš, F.; Achelle, S.; Barsella, A.; Kvashnin, Y.A.; Rusinov, G.L.; Charushin, V.N. Push–Pull Derivatives Based on 2,4′-Biphenylene Linker with Quinoxaline, [1,2,5]Oxadiazolo[3,4-B]Pyrazine and [1,2,5]Thiadiazolo[3,4-B]Pyrazine Electron Withdrawing Parts. *Molecules* **2022**, *27*, 4250. [CrossRef]
22. Aguilar-Martínez, M.; Cuevas, G.; Jiménez-Estrada, M.; González, I.; Lotina-Hennsen, B.; Macías-Ruvalcaba, N. An Experimental and Theoretical Study of the Substituent Effects on the Redox Properties of 2-[(R-phenyl)amine]-1,4-naphthalenediones in Acetonitrile. *J. Org. Chem.* **1999**, *64*, 3684–3694. [CrossRef] [PubMed]
23. Hodgson, J.L.; Namazian, M.; Bottle, S.E.; Coote, M.L. One-Electron Oxidation and Reduction Potentials of Nitroxide Antioxidants: A Theoretical Study. *J. Phys. Chem. A* **2007**, *111*, 13595–13605. [CrossRef] [PubMed]
24. Ribeiro da Silva, M.D.M.C.; Gomes, J.R.B.; Gonçalves, J.M.; Sousa, E.A.; Pandey, S.; Acree, W.E. Thermodynamic Properties of Quinoxaline-1,4-Dioxide Derivatives: A Combined Experimental and Computational Study. *J. Org. Chem.* **2004**, *69*, 2785–2792. [CrossRef] [PubMed]
25. Lauria, A.; Almerico, A.M.; Barone, G. The influence of substitution in the quinoxaline nucleus on 1,3-dipolar cycloaddition reactions: A DFT study. *Comput. Theor. Chem.* **2013**, *1013*, 116–122. [CrossRef]
26. Mishra, A.; Verma, C.; Srivastava, V.; Lgaz, H.; Quraishi, M.A.; Ebenso, E.E.; Chung, I.-M. Chemical, Electrochemical and Computational Studies of Newly Synthesized Novel and Environmental Friendly Heterocyclic Compounds as Corrosion Inhibitors for Mild Steel in Acidic Medium. *J. Bio Tribo Corros.* **2018**, *4*, 32. [CrossRef]
27. Miller, E.M.; Brazel, C.J.; Brillos-Monia, K.A.; Crawford, P.W.; Hufford, H.C.; Loncaric, M.R.; Mruzik, M.N.; Nenninger, A.W.; Ragain, C.M. Reduction Potential Predictions for Some 3-Aryl-Quinoxaline-2-Carbonitrile 1,4-Di-N-Oxide Derivatives with Known Anti-Tumor Properties. *Computation.* **2019**, *7*, 6. [CrossRef]
28. Hu, Y.; Xia, Q.; Shangguan, S.; Liu, X.; Hu, Y.; Sheng, R. Synthesis and biological evaluation of 3-aryl-quinoxaline-2-carbonitrile 1,4-di-N-oxide derivatives as hypoxic selective anti-tumor agents. *Molecules* **2012**, *17*, 9683–9696. [CrossRef]
29. Hay, P.J.; Wadt, W.R. Ab initio effective core potentials for molecular calculations—Potentials for K to Au including the outermost core orbitals. *J. Chem. Phys.* **1985**, *82*, 299–310. [CrossRef]
30. Ditchfield, R.; Hehre, W.J.; Pople, J.A. Self-Consistent Molecular Orbital Methods. 9. Extended Gaussian-type basis for molecular-orbital studies of organic molecules. *J. Chem. Phys.* **1971**, *54*, 724. [CrossRef]
31. Pooladian, F.; Crawford, P.W.; Kessler, J.M.; Casey, G.R.; Ragain, C.M. Reduction Potential for Some 1,4-Di-N-oxide quinoxaline-2-car-boxamide derivatives with anti-tuberculosis activity. *Compounds* **2023**, *3*, 83–95. [CrossRef]
32. Dunning, T.H. Gaussian basis sets for use in correlated molecular calculations. I. The atoms boron through neon and hydrogen. *J. Chem. Phys.* **1989**, *90*, 1007–1023. [CrossRef]
33. Miller, M.E.; Xia, Q.; Cella, E.M.; Nenninger, W.A.; Mruzik, N.M.; Brillos-Monia, A.K.; Hu, Z.Y.; Sheng, R.; Ragain, M.C.; Crawford, P.W. Voltammetric Study of Some 3-Aryl-quinoxaline-2-carbonitrile 1,4-di-N-oxide Derivatives with Anti-Tumor Activities. *Molecules* **2017**, *22*, 1442. [CrossRef] [PubMed]
34. Bartlett, R.J.; Musial, M. Coupled-cluster theory in quantum chemistry. *Rev. Mod. Phys.* **2007**, *79*, 291–352. [CrossRef]
35. Dennington, R.; Keith, T.; Millam, J. *Millam GaussView, Version 5*; Semichem Inc.: Shawnee Mission, KS, USA, 2016.
36. Frisch, M.J.; Trucks, G.W.; Schlegel, H.B.; Scuseria, G.E.; Robb, M.A.; Cheeseman, J.R.; Scalmani, G.; Barone, V.; Petersson, G.A.; Nakatsuji, H.; et al. *Gaussian 09, Revision D.01*; Gaussian, Inc.: Wallingford, CT, USA, 2016.